INSTITUTE OF PHYSICS PUBLISHING PHYSICS IN MEDICINE AND BIOLOGY

Phys. Med. Biol. **51** (2006) 6141–6156 doi:10.1088/0031-9155/51/23/014

Cell model for efficient simulation of wave propagation in human ventricular tissue under normal and pathological conditions

K H W J Ten Tusscher and A V Panfilov

Department of Theoretical Biology, Utrecht University, Padualaan 8, 3584 CH Utrecht, The Netherlands

E-mail: khwjtuss@hotmail.com

Received 12 July 2006, in final form 22 October 2006
Published 9 November 2006
Online at stacks.iop.org/PMB/51/6141

Abstract

In this paper, we formulate a model for human ventricular cells that is efficient enough for whole organ arrhythmia simulations yet detailed enough to capture the effects of cell level processes such as current blocks and channelopathies. The model is obtained from our detailed human ventricular cell model by using mathematical techniques to reduce the number of variables from 19 to nine. We carefully compare our full and reduced model at the single cell, cable and 2D tissue level and show that the reduced model has a very similar behaviour. Importantly, the new model correctly produces the effects of current blocks and channelopathies on AP and spiral wave behaviour, processes at the core of current day arrhythmia research. The new model is well over four times more efficient than the full model. We conclude that the new model can be used for efficient simulations of the effects of current changes on arrhythmias in the human heart.

1. Introduction

Sudden cardiac death is a major cause of death in the industrialized western world. In a majority of the cases sudden cardiac death is caused by the occurrence of a cardiac arrhythmia called ventricular fibrillation. Despite the fact that cardiac arrhythmias have been studied for over half a century, the precise mechanisms causing and sustaining fibrillation are still poorly understood.

Mathematical models and computer simulations play an increasingly important role in cardiac arrhythmia research. Major advantages of computer simulations are the ability to study wave propagation in the 3D cardiac wall, which is currently still impossible in experiments, and the ability to bridge the gap between changes in ionic currents and ion channel mutations at a sub-cellular and cellular level and arrhythmias that occur at the whole organ level. A

further important application of modelling is studying arrhythmias in the human heart, given the limited possibilities for experimental and clinical research on human hearts.

To be able to study human whole heart arrhythmia dynamics and how these are linked to (sub)cellular processes such as ion channel mutations, a human cardiac cell model that is both detailed and computationally efficient is needed. Second generation ionic models (Luo and Rudy 1994, Noble *et al* 1998, Winslow *et al* 1999, Rice *et al* 1999, Iyer *et al* 2004) contain a lot of electrophysiological detail, but are computationally very expensive, whereas phenomenological models such as FitzHugh–Nagumo like models (FitzHugh 1960, 1961, Nagumo *et al* 1962, Aliev and Panfilov 1996) and the Fenton–Karma model (Fenton and Karma 1998) are computationally very efficient, but lack electrophysiological detail. We therefore need a model of an intermediate type.

Bernus *et al* (2002) constructed a relatively simple ionic model for human ventricular cells based on the second generation Priebe–Beuckelmann ionic model (Priebe and Beuckelmann 1998). The disadvantage of this intermediate-type model is that the Priebe–Beuckelmann model itself is based on only a limited amount of at that time available human cardiac cell data. Therefore, the main aim of this paper is to formulate a new intermediate-type model for human ventricular cells. In the first part of our paper we derive this new model from our recently published detailed human ventricular cell model (Ten Tusscher and Panfilov 2006, Ten Tusscher *et al* 2004), using a similar approach as followed in Bernus *et al* (2002).

The second part of our paper consists of a careful comparison of the behaviour of our reduced and full model in single cell, cable and two-dimensional settings to validate that both models behave in the same manner. We show that our reduced model has a similar action potential shape, duration and restitution, can reproduce different cell types, can reproduce the consequences of I_{Ks} and I_{Kr} current block and can reproduce the effects of genetic mutations such as the LQT-3 and Brugada syndrome. We demonstrate that our reduced model has similar conduction velocity restitution and has similar spiral wave dynamics and stability as our full model.

Finally, we demonstrate that our reduced model is well over four times more efficient than our full human ventricular cell model. This speedup can be crucial for making ionic whole organ simulations achievable without the use of supercomputers or very large clusters. Without the speedup, performing whole organ simulations within a reasonable run time would require the use of around 100 parallel processors. With the speedup, reasonable run times can be achieved using affordable 10–20 processor parallel clusters.

2. Materials and methods

2.1. Model development

2.1.1. Intracellular sodium and potassium concentrations. Similar to the approach followed in Bernus *et al* (2002) we treat intracellular sodium and potassium concentrations as constant-valued model parameters rather than variables. The rationale behind this approach is that intracellular sodium and potassium concentrations hardly change over the duration of a few action potentials. Significant changes in sodium and potassium concentrations, such as occur under conditions of ischaemia or hyperkalaemia, occur over timescales of several minutes (Boyett and Fedida 1988). Such timescales are far beyond the timescales that are currently computed in whole heart arrhythmia simulations.

2.1.2. Intracellular calcium concentrations and calcium release. Intracellular calcium concentrations change significantly during each action potential. These dynamics are essential

for cardiac contraction and feed back on cardiac excitation by influencing ionic currents such as the L-type calcium channel and the sodium calcium exchanger. The influence of calcium dynamics on cardiac excitation is of particular importance when studying conditions such as calcium overload, spontaneous calcium release and calcium-induced alternans. However, when not studying these particular conditions, AP morphology, duration, restitution and propagation can very well be reproduced using a model that does not incorporate calcium handling (Bernus *et al* 2002). We therefore decided to remove intracellular calcium dynamics from our model, and treat calcium as a constant-valued parameter.

Now we can also remove the subspace calcium inactivation gate (f_{cass}) and the $\mathrm{Ca_{ss}}$ dependent driving force from our L-type calcium current description. This results in an L-type calcium current description with only voltage dependent gates, similar to I_{CaL} in Bernus *et al* (2002), Luo and Rudy (1991), Zhang *et al* (2000). To compensate for the absence of f_{cass} and obtain similar inactivation dynamics for I_{CaL} in the reduced and full model we adjusted the time dynamics of the fast voltage inactivation gate (f_2). The new equations for I_{CaL} are:

$$I_{\mathrm{CaL}} = G_{\mathrm{CaL}} \mathrm{d} f f_2 (V - 60) \tag{1}$$

$$f_{2\infty} = \frac{0.67}{1 + \mathrm{e}^{(V+35)/7}} + 0.33 \tag{2}$$

$$\alpha_{f2} = 600\,\mathrm{e}^{-\frac{(V+27)^2}{170}} \tag{3}$$

$$\beta_{f2} = \frac{7.75}{1 + \mathrm{e}^{(25-V)/10}} \tag{4}$$

$$\gamma_{f2} = \frac{16}{1 + \mathrm{e}^{(V+30)/10}} \tag{5}$$

$$\tau_{f2} = \alpha_{f2} + \beta_{f2} + \gamma_{f2}. \tag{6}$$

Removing intracellular calcium dynamics significantly increases the computational efficiency of our model, as it reduces the number of variables by five ($\mathrm{Ca_{ss}}$, $\mathrm{Ca_i}$, $\mathrm{Ca_{SR}}$, R, f_{cass}) and the number of equations by 25 (intracellular calcium fluxes, buffering and reversal potentials).

2.1.3. Simplifying ionic currents. To further reduce the number of variables, we use quasi-steady-state approximations for some of the fast changing current gating variables, similar to the approach followed in Bernus *et al* (2002). Fast changing gates in our model are: the m gate of I_{Na}, the r gate of I_{to}, the x_{r2} gate of I_{Kr} and the d gate of I_{CaL}.

For I_{to}, I_{Kr} and I_{CaL} using a steady-state approximation for the r, x_{r1} and d gates can be done without significant changes of the AP or conduction properties of the model. However, using a quasi-steady-state approximation for the I_{Na} m gate has significant consequences for action potential upstroke velocity, conduction velocity and conduction velocity restitution. Therefore, we decided to keep the I_{Na} m gate as a model variable.

The new equations for I_{to}, I_{Kr} and I_{CaL} become

$$I_{\mathrm{to}} = G_{\mathrm{to}} r_\infty(V) s (V - E_K) \tag{7}$$

$$I_{\mathrm{Kr}} = G_{\mathrm{Kr}} x_{r1} x_{r2\infty}(V)(V - E_K) \tag{8}$$

$$I_{\mathrm{CaL}} = G_{\mathrm{CaL}} d_\infty(V) f f_2 (V - 60). \tag{9}$$

This further reduces our model with three variables. In total we removed ten variables, leaving nine variables in our reduced model.

Table 1. Parameter values in the full and reduced model for the default and steep settings. If parameter values are not mentioned, they have been left unchanged from the default setting of the full model and can be found in Ten Tusscher and Panfilov (2006). Concentrations are in mM, conductances are in nS pF^{-1}, except for L-type calcium conductance in the full model which is in cm $ms^{-1}\mu F^{-1}$, due to the Goldmann–Hodgkin–Katz formulation for the driving force. For the steep setting, τ_f was multiplied by a factor 2 for the voltage range $V > 0$, to slow down inactivation but not recovery dynamics.

Setting	Parameter	Full model	Reduced model
All	Nai	Variable	7.67
	Ki	Variable	138.3
	Cai	Variable	0.000 07
	G_{CaL}	3.980^{-5}	0.2786
Default	G_{Kr}	0.153	0.101
	G_{Ks}	0.392	0.257
	G_{pK}	0.0146	0.0293
Steep	G_{Kr}	0.172	0.126
	G_{Ks}	0.441	0.321
	G_{pK}	0.002 19	0.002 19
	G_{pCa}	0.8666	1.238
	τ_f	$\times 2$	$\times 2$

2.1.4. Parameter adjustments. To obtain a similar action potential shape and duration characteristics for the full and reduced model, a number of parameter values were adjusted. In table 1 parameter values for I_{CaL}, I_{Kr}, I_{Ks} and I_{pK} conductance in the full and reduced model are shown for the default setting of both models. It should be noted that for all changed parameters the values in the reduced model are within the same order of magnitude as in the full model. Furthermore, both the parameter values in the full model and in the reduced model are within the range of values found experimentally for ventricular cells. Other current characteristics, such as activation, inactivation and I, V curves were left unchanged from the full model (Ten Tusscher and Panfilov 2006, Ten Tusscher *et al* 2004). All other parameter values were unchanged from the full to the reduced model.

Given the small number of parameters changed, and the relatively small changes in parameter values, we hypothesize that the relative importance of the different ionic currents should be similar in the full and reduced model. This will be tested in subsequent sections.

2.2. Numerical methods

Action potential generation and propagation was described using the following differential equation (Keener and Sneyd 1998):

$$C_m \frac{\partial V}{\partial t} = I_{ion} + I_{stim} + D\Delta V \tag{10}$$

where C_m is the membrane capacitance, V is the transmembrane potential, I_{stim} is the externally applied transmembrane current, I_{ion} is the sum of all transmembrane ionic currents and D is the diffusion coefficient. For I_{ion} we use either our new human ventricular cell model (Ten Tusscher and Panfilov 2006), or the reduced version of this model which was described in the previous section. For D we use $D = 0.001\,54$ cm^2 ms^{-1} in 1D and 2D simulations to obtain a maximum planar conduction velocity (CV) of 68 cm s^{-1} consistent with measurements in human ventricular tissue (Taggart *et al* 2000), and a value of $D = 0$ cm^2 ms^{-1} for single cells.

Table 2. Dependence of conduction velocity (CV) and action potential duration (APD) on time step (Δt) of integration for a space step $\Delta x = 0.025$ mm.

Model	Δt (ms)	CV (cm s^{-1})	APD (ms)
Full	0.04	66.2	310
	0.02	68.7	310
	0.01	70.0	310
	0.005	70.7	310
Reduced	0.04	63.0	314
	0.02	65.0	312
	0.01	66.1	312
	0.005	66.7	313

Table 3. Dependence of conduction velocity (CV) and action potential duration (APD) on space step (Δx) of integration for a time step $\Delta t = 0.02$ ms.

Model	Δx (mm)	CV (cm s^{-1})	APD (ms)
Full	0.040	63.0	310
	0.025	68.7	310
	0.015	72.6	310
Reduced	0.040	58.9	312
	0.025	65.0	312
	0.015	69.2	313

Physical units used in our model are as follows, time (t) in milliseconds, voltage (V) in millivolts, current densities (I_X) in picoamperes per picofarad and ionic concentrations (X_i, X_o) in millimoles per litre.

For single cell simulations, forward Euler integration with a time step of $\Delta t = 0.02$ ms was used to integrate equation (10) . For 1D and 2D computations, the forward Euler method was used to integrate equation (10) with a space step of $\Delta x = 0.25$ mm and a time step of $\Delta t = 0.02$ ms. In all cases the Rush and Larsen integration scheme (Rush and Larsen 1978) was used to integrate the Hodgkin–Huxley-type equations for the gating variables.

We test the accuracy of our numerical simulations in a cable of cells by varying the time and space step of integration (tables 2 and 3). We see similar results for the full and reduced model. From table 2 we can see that for a space step of $\Delta x = 0.25$ mm decreasing Δt from 0.02 ms to 0.005 ms leads to a 2–3% increase in CV and a 0–0.3% increase in action potential duration (APD). From table 3 we can see that for a time step of $\Delta t = 0.02$ ms decreasing Δx from 0.025 mm to 0.015 mm leads to a $\sim$6% increase in CV and a 0–0.3% increase in APD. These changes are similar to those reported for other models (see, for example, Qu *et al* (1999)). Throughout the rest of this paper we use a time step of $\Delta t = 0.02$ ms and a space step of $\Delta x = 0.2$ mm, similar to values used in other studies (Qu *et al* 1999, Cao *et al* 1999, Xie *et al* 2001, Bernus *et al* 2002).

In single cells, we use the dynamic protocol to determine action potential duration restitution. We apply a series of 50 stimuli at a specified BCL, following which cycle length is decreased. The APD restitution curve is obtained by plotting the final APD for each BCL against the final DI. In cables, we apply the dynamic restitution protocol to determine conduction velocity (CV) restitution. We do so by pacing one end of the 800 cells long cable at a certain BCL until a steady state APD and CV are reached, after which the cycle length is decreased.

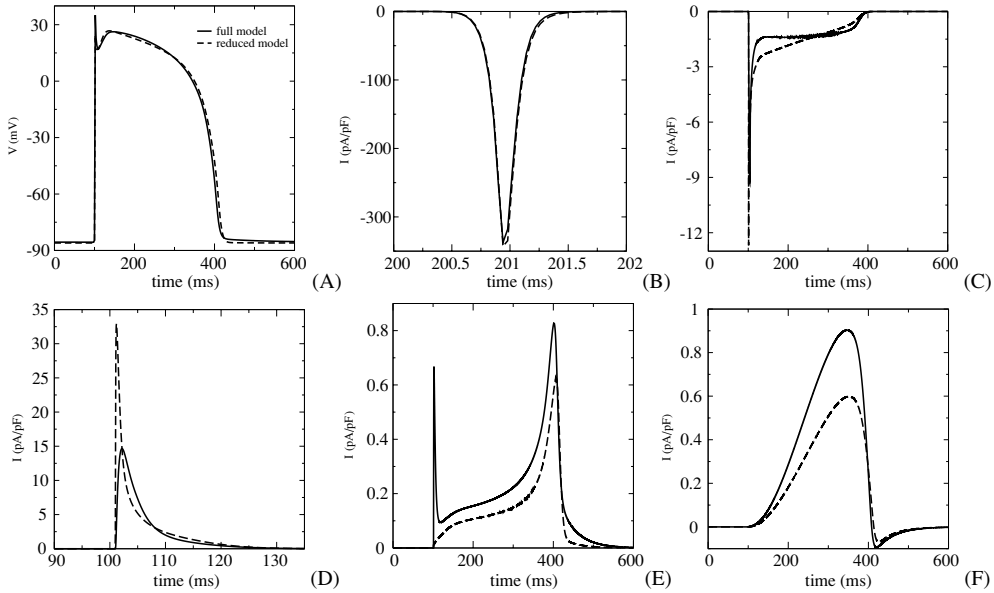

Figure 1. Steady state 1 Hz action potential and major ionic currents of the full and reduced model. (A) Action potential. (B) Fast sodium current. Note the difference in time scale relative to the other figures. (C) L-type calcium current. (D) Transient outward current. Note the difference in time scale relative to the other figures. (E) Rapid delayed rectifier potassium current. (F) Slow delayed rectifier potassium current.

We use two-dimensional tissue sheets of 1000×1000 cells (space step $\Delta x = 0.25$ mm). In 2D spiral waves are generated by first applying an S1 stimulus producing a planar wavefront propagating in one direction, then, when the refractory tail of this wave crosses the middle of the medium, an S2 stimulus is applied generating a second wavefront perpendicular to the first. This produces a wavefront with a free end around which it curls, forming a spiral wave. Stimulus currents lasted for 2 (S1) and 5 (S2) ms and were twice the diastolic threshold. Phase singularities (PS), the points around which spiral waves rotate, are detected by intersecting an isopotential line (-60 mV) and the $dV/dt = 0$ line (Fenton and Karma 1998).

Simulations were coded in C^{++} and run on a single processor of a Dell 650 Precision Workstation (dual Intel xeon 2.66 GHz).

3. Results

3.1. Normal electrophysiological properties

3.1.1. Action potential and ionic currents. In figure 1 we show a steady state (epicardial) AP and the major ionic currents contributing to this action potential at 1 Hz pacing for our full and reduced model. In figure 1(A) we can see that AP shape is almost identical in the full and reduced model. The resting potential is -85.6 mV in the full and -86.0 mV in the reduced model, $\dot{V}_{\max} = 292$ V s^{-1} in the full and $\dot{V}_{\max} = 297$ V s^{-1} in the reduced model. Amplitude and shape of the fast sodium current are similar for the full and reduced model (figure 1(B)). In figure 1(C) we can see that the dynamics of I_{CaL} in the full and reduced model are qualitatively similar: both show a first phase of fast activation and fast partial inactivation

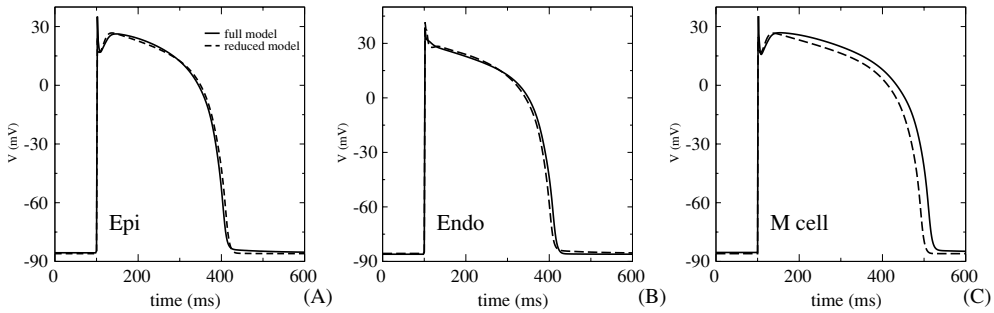

Figure 2. Steady state 1 Hz action potential morphology for epicardial (A), endocardial (B) and M cells (C) in the full and reduced model. See the text for details on the differences in parameter settings between the cell types.

and a second phase of slower inactivation. However, there are some quantitative differences: in the full model the calcium current inactivates to a relatively constant plateau level until final inactivation, whereas in the reduced model the calcium current gradually decreases during the AP plateau phase.

I_{to} shape and duration are also somewhat different in the full and reduced model (figure 1(D)). However, the integral of the I_{to} current in the two models is very similar, resulting in a similar effect of I_{to} current on AP shape. In figure 1(E) we see a qualitatively similar shape of I_{Kr} current, except for the initial peak. This peak is absent in the reduced model due to the instantaneous rather than time dependent inactivation of I_{Kr} ($x_{r2\infty}$), as is the case in most models (Zeng *et al* 1995, Priebe and Beuckelmann 1998, Courtemanche *et al* 1998, Iyer *et al* 2004). In addition the I_{Kr} current in the reduced model has a slightly smaller amplitude as in the full model. In figure 1(F) we can see that the I_{Ks} current has a similar shape and slightly smaller amplitude as in the full model. The smaller I_{Kr} and I_{Ks} current amplitudes are due to a smaller conductance in the reduced model (see table 1), which were necessary to obtain the same APD as in the full model.

3.1.2. Three different cell types. Using both the full and the reduced model we are able to simulate the three different cell types found across the ventricular wall (Drouin *et al* 1995, Li *et al* 1998). Figure 2 shows steady state epicardial (A), endocardial (B) and M cell (C) action potentials for the full and reduced model for a BCL of 1000 ms. Epicardial cells are simulated by using the standard parameter setting of our full (Ten Tusscher and Panfilov 2006) and reduced (table 1) model. Endocardial cells differ from epicardial cells in their 75% lower I_{to} density, and in their slower recovery from inactivation of the I_{to} current (Ten Tusscher *et al* 2004), leading to a virtual absence of the AP notch. These differences are based on data from (Nabauer *et al* 1996, Wettwer *et al* 1994). In our model M cells differ from epicardial cells only in having a 75% lower I_{Ks} density (Pereon *et al* 2000), leading to a longer AP duration, similar to our approach in (Ten Tusscher *et al* 2004).

We can see that epicardial, endocardial and M cell action potentials are very similar both in duration and morphology in the full compared to the reduced model.

3.1.3. APD and CV restitution. The APD and CV restitution curves describe how action potential duration and action potential propagation speed change as a function of the duration of the diastolic interval between the current and preceding action potential. It has been

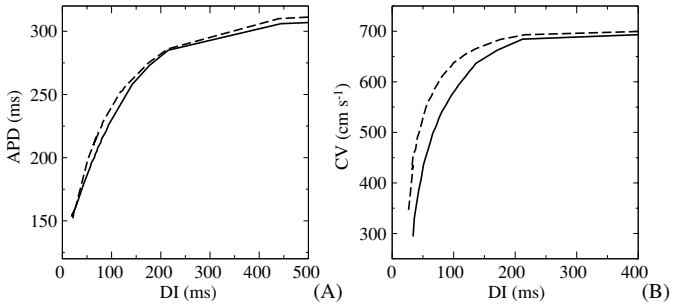

Figure 3. Restitution properties of the full and reduced model. (A) Dynamic action potential duration restitution. (B) Conduction velocity restitution.

extensively demonstrated (Panfilov and Holden 1990, Karma 1993, Karma 1994, Qu *et al* 1999, Cao *et al* 1999, Cherry and Fenton 2004, Ten Tusscher and Panfilov 2006) that action potential duration and conduction velocity restitution properties are of critical importance for determining what kind of reentrant arrhythmia will occur, i.e. whether stable spiral wave rotation or spiral breakup will occur. Therefore, our reduced model should have realistic APD and CV restitution properties.

In figure 3(A) we can see that the full and reduced model have very similar dynamic APD restitution properties. Note that the restitution properties of our full model have been fitted to reproduce recently measured human restitution curves (Nash *et al* 2006, Ten Tusscher and Panfilov 2006). In figure 3(B) we can see that the full and reduced model have a qualitatively similar, gradually declining CV restitution curve. Quantitatively, CV in the full model starts decreasing for slightly longer DIs than in the reduced model, resulting in somewhat lower conduction velocities for the shortest DIs. However, these small differences turn out not to have a significant effect on spiral wave dynamics and stability (see figure 7).

3.2. Effect of current blocks and channelopathies

3.2.1. I_{Ks}, I_{Kr}, I_{to} and I_{CaL} block. The main aim of this study was to develop a model that is computationally efficient yet maintains a lot of detailed characteristics for the major ionic currents. Here we check whether our reduced model produces the correct responses to I_{Kr}, I_{Ks}, I_{to} and I_{CaL} current block.

Figure 4 shows a normal AP, and APs when I_{Kr} or I_{Ks} current is fully blocked. We can see that both blocks result in an increase of APD. Normal APD is 315 ms, APD under I_{Kr} block is 355 ms, an increase of 40 ms or 12.7%, similar to experiments reporting an increase of 6% (88 ms) (Li *et al* 1996) and 11% (47 ms) (Iost *et al* 1998) upon full I_{Kr} block. APD under I_{Ks} block is 467 ms, an increase of 152 ms or 48.3%, similar to experiments reporting an APD prolongation of approximately 40% (140 ms) upon full I_{Ks} block (Bosch *et al* 1998). These results are also very similar to results for the first version of our full human ventricular cell model (Ten Tusscher *et al* 2004, TenTusscher and Panfilov 2004).

Figure 5 shows a normal AP, an AP when I_{to} current is fully blocked, and an AP when I_{CaL} current is fully blocked in both the full (figure 5(A)) and reduced (figure 5(B)) model. As expected we see that block of I_{to} results in the absence of the epicardial AP notch, and that block of I_{CaL} results in a significant shortening of APD. I_{to} and I_{CaL} block have very similar effects on APD and AP shape in the reduced and full model.

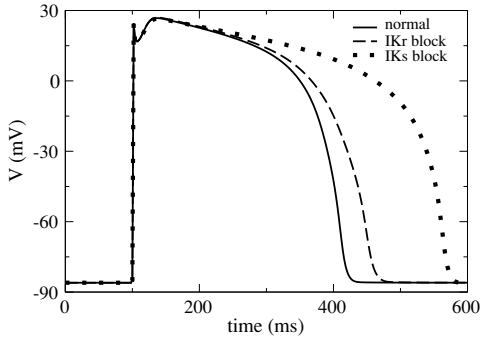

Figure 4. Steady state 1 Hz action potentials in the reduced model for the normal parameter setting, for 100% I_{Kr} current block and for 100% I_{Ks} current block.

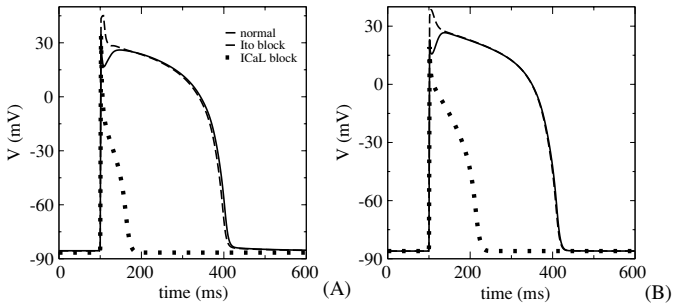

Figure 5. Steady state 1 Hz action potentials in the full (A) and reduced (B) model for the normal parameter setting, for 100% I_{to} current block and for 100% I_{CaL} current block.

3.2.2. LQT-3 and Brugada syndrome. Here we investigate whether our reduced model can be used to study the LQT-3 syndrome and the Brugada syndrome.

LQT-3 syndrome. LQT-3 syndrome is caused by mutations in the SCN5A gene coding for the fast sodium channel (Grant 2001, Rivolta *et al* 2001) that lead to a partial loss or slowing of inactivation of the fast sodium current. We simulated a case of LQT-3 syndrome in which I_{Na} inactivation is incomplete, by adjusting the steady-state functions of the inactivation gates h and j of I_{Na}:

$$h_{\infty\,\text{wild type}} = j_{\infty\,\text{wild type}} = \frac{1}{(1+\mathrm{e}^{(V+71.55)/7.43})^2} \tag{11}$$

$$h_{\infty\,\text{LQT-3}} = j_{\infty\,\text{LQT-3}} = \frac{(1-l)}{(1+\mathrm{e}^{(V+71.55)/7.43})^2} + l \tag{12}$$

where the fraction describes the inactivating part of I_{Na} (100% in the wildtype $(100-100l)\%$ in the LQT-3 mutant), and l represents the non-inactivating part of I_{Na} responsible for $I_{Na,late}$. In figures 6(A) and (B) we simulated LQT-3 syndrome in M cells in both our full and reduced model at a BCL = 1250 or 1750 ms. We used values of $l = 0.0305$ for the full model and $l = 0.025$ for the reduced model in figure 6(A), resulting in $I_{Na,late}$ amplitudes of 3.05% and 2.5% of peak I_{Na} amplitude, respectively. In figure 6(B) we used $l = 0.0315$ for the full model and $l = 0.026$ for the reduced model, resulting in $I_{Na,late}$ amplitudes of 3.15% and 2.6% of peak I_{Na} amplitude, respectively. These LQT-3 $I_{Na,late}$ amplitudes are in the range of

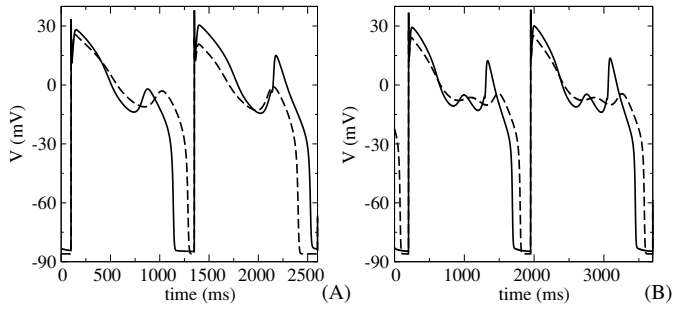

Figure 6. M cells and LQT-3 syndrome in the full and reduced model. (A) LQT-3 M cell action potentials with a single EAD at a BCL = 1250 ms. (B) LQT-3 M cell action potentials with multiple EADs at a BCL = 1750 ms. See the text for a full description of M cells and LQT-3 syndrome parameter settings. Note that EADs also occurred under these parameter settings for BCL = 1000 ms, but that this leads to interference between the prolonged EAD and the next stimulus. We therefore decided to display EADs at slightly longer BCL for clarity.

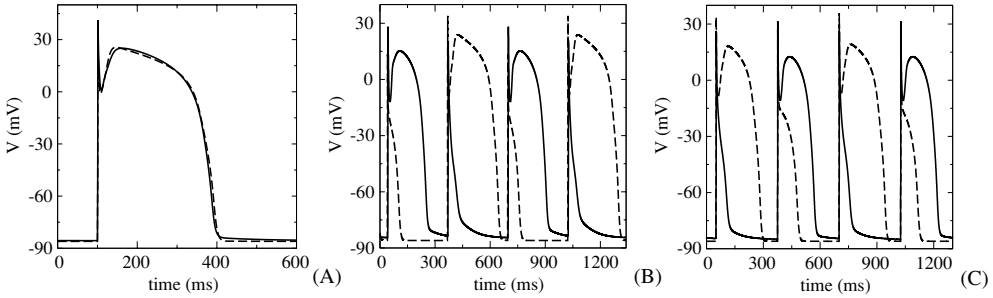

Figure 7. Epicardial cells with a deep notch and the Brugada syndrome in the full and reduced model. (A) Epicardial action potentials with a deep notch (BCL = 1000 ms). (B) Brugada syndrome: short triangular and long 'coved dome' shaped APs as a result of an I_{to} increase of function mutation (BCL = 328 ms). (C) Brugada syndrome: short and long APs as a result of an I_{CaL} decrease of function mutation (BCL = 325 ms). See the text for a detailed description of deep-notch epicardial cell and Brugada syndrome parameter settings.

experimentally found values (Wei *et al* 1999, Keller *et al* 2003). We see that for approximately the same percentage of non-inactivating I_{Na} we get the same type and number of EADs in both our full and reduced model.

Brugada syndrome. Brugada syndrome is characterized by the occurrence of both very short, triangular and prolonged, 'coved dome' shaped APs at short BCL (Dumaine *et al* 1999). The short APs occur as a result of complete repolarization during the AP notch, whereas the long APs occur as a result of a deep and long lasting AP notch leading to an increase in AP plateau duration. Epicardial cells with a large I_{to} current and deep AP notch are particularly prone to developing Brugada characteristics (Clancy and Rudy 2002, Fish and Antzelevitch 2003). So far, Brugada syndrome has only been linked to mutations in the SCN5A gene, which lead to a reduction of fast sodium current (Antzelevitch 1999). However, mutations leading to an increase in I_{to} or a decrease in I_{CaL} current are likely candidates for Brugada syndrome in patients where no mutations in SCN5A are found (Antzelevitch 1999).

In figure 7(A) we simulated an epicardial AP with a deep notch in both our full and reduced model. This cell type was constructed by shifting the half-activation potential of the I_{to} r gate from $V_{1/2} = 20$ mV to $V_{1/2} = 2.5$ mV for the full and to $V_{1/2} = -5$ mV for the

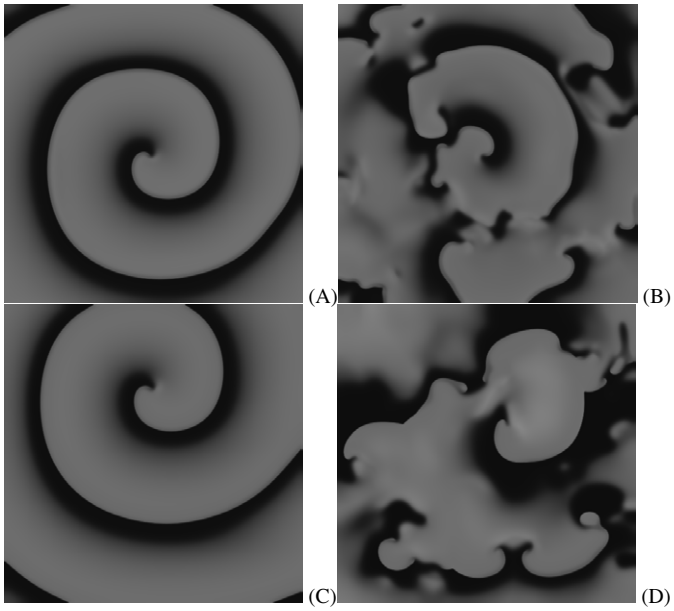

Figure 8. Spiral wave dynamics. (A) Stable spiral wave dynamics in the full model for a setting with an APD restitution slope slightly steeper than one. (B) Spiral breakup in the full model for a setting with an APD restitution slope considerably over one. (C) Stable spiral wave dynamics in the reduced model for a setting with an APD restitution slope slightly over one. (D) Spiral breakup in the reduced model for a setting with a restitution slope considerably over one.

reduced model, leading to a larger amplitude and faster activation of I_{to}. In figure 7(B) we simulated a hypothesized Brugada syndrome mutation leading to a gain of function in the I_{to} current by increasing G_{to} with 27% in the full and 44% in the reduced model. In both models we see the interchange of short triangular APs and long 'coved dome' APs typical for Brugada syndrome. In figure 6(C) we simulated a hypothesized Brugada syndrome mutation leading to a loss of function in the I_{CaL} current, by reducing G_{CaL} with 35% in both the full and the reduced model. Again we see the interchange of long and short APs in both models.

3.3. 2D propagation and computational efficiency

3.3.1. Spiral wave dynamics. Figure 8 shows spiral wave dynamics for our full model (top row) and reduced model (bottom row) for the default parameter settings of both models which results in an APD restitution slope slightly over one (1.1) (left column) and for an alternative setting which results in a restitution slope considerably steeper than one (1.8) (right column). (For parameter settings see (Ten Tusscher and Panfilov 2006) and table 1.) We can see that for both models, the default parameter setting results in stable spiral wave rotation and the steep parameter setting results in spiral breakup.

To further compare spiral wave dynamics in the full and reduced model, we determined spiral wave meander pattern, rotation period and frequency spectrum for the stable spiral waves shown in figures 8(A) and (B). Figures 9(A) and (B) show spiral tip meander patterns for the full and reduced model. We see that both the shape (circular) and size of the meander patterns are very similar. For stable spiral wave rotation we find a period of 192 ms in the full model and a period of 200 ms in the reduced model. In figure 9(C) and (D) we show frequency spectra of electrical activity recorded in point (400, 400) during spiral wave rotation. We can

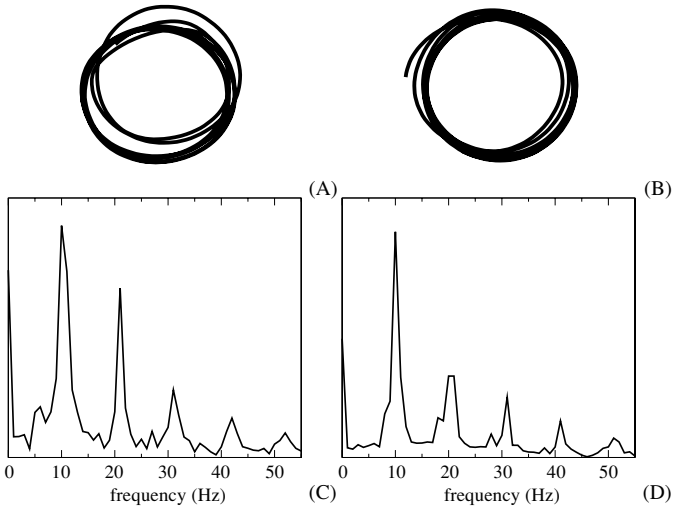

Figure 9. Spiral wave dynamics, continued. (A) Stable spiral wave meander pattern in the full model. (B) Stable spiral wave meander pattern in the reduced model. (C) Frequency spectrum of electrical activity in point (400, 400) during stable spiral wave rotation in the full model. (C) Frequency spectrum of electrical activity in point (400, 400) during stable spiral wave rotation in the reduced model.

see that the frequency spectra in the full and reduced model look very similar. We conclude that spiral wave dynamics in the reduced model closely resemble spiral dynamics in the full model.

An important question is whether our reduced model is able to reproduce the experimental finding that reducing I_{CaL} flattens APD restitution and stops fibrillation (Riccio *et al* 1999, Koller *et al* 2000, Garfinkel *et al* 2000). To determine this we started with the steep parameter setting (figure 8(D)) and gradually decreased G_{CaL} (figure 10(A)) and hence restitution slope (figure 10(B)). Figure 8(D) shows spiral wave dynamics 4 s after the start of the simulation, when G_{CaL} and restitution slope are (still) at their maximal value, full blown spiral breakup has developed and a total of 18 phase singularities (PS) are present. In figures 10(C) and (D) we show spiral wave dynamics 7 s and 9 s after the start of the simulation. At 7 s, when G_{CaL} has been decreased to approximately 30% of its original value, the number of spiral waves present is significantly reduced (4 PS). At 9 s, when G_{CaL} has been decreased to ∼20% of its original value, spiral breakup has stopped and a single stable spiral wave remains (1 PS). So despite the absence of intracellular calcium dynamics in our reduced model, the model correctly reproduces the effect of reducing I_{CaL} current.

3.3.2. Computational efficiency. We performed a comparison of the computer time needed to simulate 4 s of spiral wave dynamics in a 1000 × 1000 tissue sheet using either our full or reduced model (the above discussed simulations). For the full model we needed ∼7400 min and for the reduced model we needed ∼1680 min for a single 4 s simulation. Thus, using the reduced model we obtained a speedup of a factor 4.4 over the full model.

Note that the speedup is almost two times more than could be expected based on the reduction of the number of variables ($19/9 = 2.1$). This can be explained by the fact that removing all intracellular ion concentrations as variables significantly reduces the number of equations that need to be solved for the remaining variables, since for example reversal potentials and buffering fractions now have a constant value.

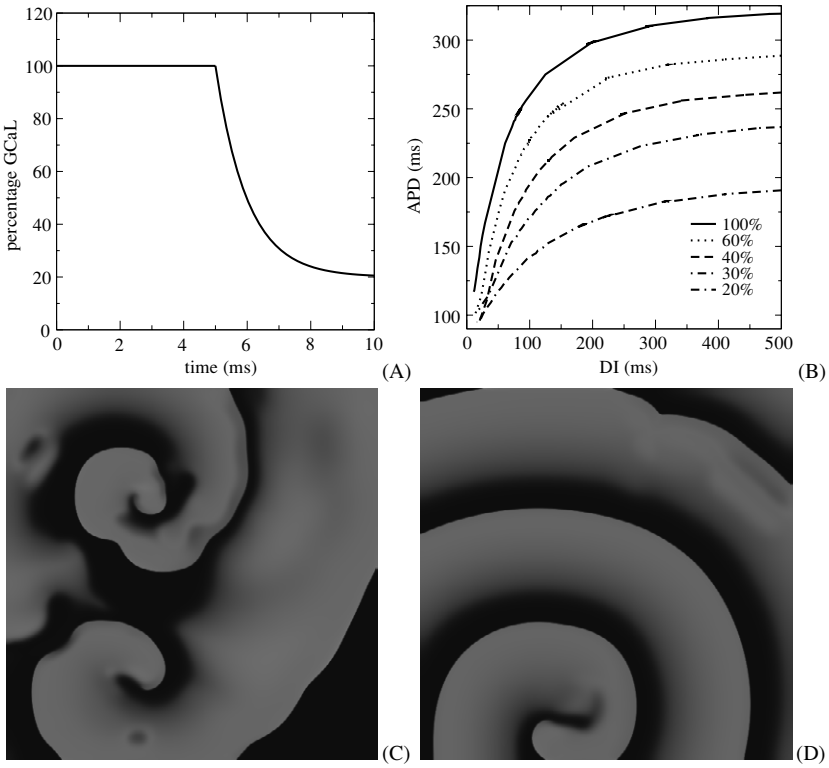

Figure 10. Influence of G_{CaL} on spiral breakup. (A) Percentage change in I_{CaL} conductance over the course of the simulation. The first 5 s G_{CaL} is left unchanged from its original, maximal value to allow full blown spiral breakup to develop. After that, G_{CaL} is gradually decreased using the function $G_{CaL} = G_{CaL}((1 - P) + Pe^{(t-T_0)/\tau})$, with $P = 0.8$, $T_0 = 5$ s and $\tau = 1$ s. (B) Dynamic APD restitution for the steep parameter setting of the reduced model (see table 1) for 100%, 60%, 40%, 30% and 20% of its normal G_{CaL} value. (C) Spiral wave dynamics 7 s after the start of the simulation. (D) Spiral wave dynamics 9 s after the start of the simulation.

For further comparison, we determined the time needed to simulate 4 s of spiral wave dynamics using the Luo–Rudy phase one model, which was 923 min. Thus our reduced human ventricular cell model is only a factor 1.8 slower than the Luo–Rudy phase one model.

4. Discussion

In this paper, we developed a reduced, computationally efficient model for human ventricular myocytes that retains the detailed characteristics of all major ionic currents. The model is intended for whole heart arrhythmia simulations in which the consequences of (sub)cellular processes such as channelopathies are investigated.

We performed a careful comparison of the behaviour of the reduced and full model in single cell, cable and 2D tissue sheet settings. We show that our reduced model has similar AP, ionic current morphology and APD restitution as the full model. We also show that our reduced model is capable of correctly reproducing characteristics of different cell types, responses to current blocks and behaviour in the presence of channelopathies. We demonstrate that our reduced model has similar CV restitution, spiral wave dynamics and spiral wave stability as our full model. Furthermore, we show that our reduced model is capable of reproducing the

experimental finding that reducing I_{CaL} current flattens restitution and reverts fibrillation to tachycardia, despite the fact that the reduced model does not incorporate calcium dynamics.

The reduced model is well over four times faster than the full model and is less than a factor 2 slower than the widely used phase one Luo–Rudy model, which does not incorporate an I_{to} current (important for Brugada syndrome), does not have a separate description for the I_{Ks} and I_{Kr} currents (important for M cells, LQT and SQT syndrome), and is intended for simulating guinea pig cardiac cells. A speedup of well over four makes ionic whole heart modelling feasible with the use of small, affordable 10–20 processor parallel clusters.

4.1. Limitations

There are several limitations to the model we developed in this paper. First, because of the absence of sodium and potassium dynamics we cannot investigate the *development* of conditions such as ischaemia and hyperkalaemia. However, the development of these conditions occurs over a timescale of minutes, which is too long for the whole heart arrhythmia simulations our model is intended for. Note that using our model we can simulate the effect of a developed condition of ischaemia or hyperkalaemia by changing the parameter values of intracellular sodium or extracellular potassium.

Second, because of the absence of intracellular calcium dynamics our model cannot be used for studying conditions such as calcium overload, spontaneous calcium release, calcium-induced alternans and the influence of calcium dynamics on wave break. Clearly, for these types of research questions the full model should be used (Ten Tusscher and Panfilov 2006).

Third, using steady-state assumptions for the fast activating gates of I_{to}, I_{Kr} and I_{CaL} causes them to activate instantaneously rather than with some time-delay. This may influence action potential upstroke characteristics, especially under conditions of reduced fast sodium current amplitude, such as during ischaemia or acidosis, when I_{to}, I_{Kr} and I_{CaL} dynamics become more important.

5. Conclusion

We formulated a computationally efficient simplified version of our detailed human ventricular cell model. The reduced model retains the essential details of all major ionic currents and is therefore capable of simulating effects of (sub)cellular processes such as I_{Kr} or I_{Ks} block, LQT-3 syndrome or Brugada syndrome. Because of its computational effectiveness, the model is very suited for studying the consequences of such conditions on whole heart arrhythmia dynamics.

Acknowledgments

This work was supported by the Netherlands Organisation for Scientific Research (NWO) through grant number 635100004 of the Research Council for Physical Sciences (EW) (K H W J ten Tusscher).

References

Aliev R R and Panfilov A V 1996 A simple two-variable model of cardiac excitation *Chaos Solitons Fractals* **7** 293–301

Antzelevitch C 1999 Ion channels and ventricular arrhythmias: cellular and ionic mechanisms underlying the Brugada syndrome *Curr. Opin. Cardiol.* **14** 274–9

Bernus O, Wilders R, Zemlin C W, Verschelde H and Panfilov A V 2002 A computationally efficient electrophysiological model of human ventricular cells *Am. J. Physiol. Heart Circ. Physiol.* **282** H2296–308

Bosch R F, Gaspo R, Busch A E, Lang H J, Li G and Nattel S 1998 Effects of chromanol 293B, a selective blocker of the slow component of the delayed rectifier K^+ current, on repolarization in human and guinea pig ventricular myocytes *Cardiovasc. Res.* **38** 441–50

Boyett M R and Fedida D 1988 A computer simulation of the effect of heart rate on ion concentrations in the heart *J. Theor. Biol.* **132** 15–27

Cao J, Qu Z, Kim Y, Wu T, Garfinkel A, Weiss J N, Karagueuzian H S and Chen P 1999 Spatiotemporal heterogeneity in the induction of ventricular fibrillation by rapid pacing, importance of cardiac restitution properties *Circ. Res.* **84** 1318–31

Cherry E M and Fenton F H 2004 Suppression of alternans and conduction blocks despite steep APD restitution: electrotonic, memory and conduction velocity effects *Am. J. Physiol. Heart Circ. Physiol.* **286** H2332–41

Clancy C E and Rudy Y 2002 Na^+ channel mutation that causes both brugada and long-QT syndrome phenotypes, a simulation study of mechanism *Circulation* **105** 1208–13

Courtemanche M, Ramirez R J and Nattel S 1998 Ionic mechanisms underlying human atrial action potential properties: insights from a mathematical model *Am. J. Physiol. Heart Circ. Physiol.* **275** H301–21

Drouin E, Charpentier F, Gauthier C, Laurent K and Le Marec H 1995 Electrophysiologic characteristics of cells spanning the left ventricular wall of human heart: evidence for the presence of M cells *J. Am. Coll. Cardiol.* **26** 185–92

Dumaine R, Towbin J A, Brugada P, Vatta M, Nesterenko D V, Nesterenko V V, Brugada J, Brugada R and Antzelevitch C 1999 Ionic mechanisms responsible for the electrocardiographic phenotype of the Brugada syndrome are temperature dependent *Circ. Res.* **85** 803–9

Fenton F and Karma A 1998 Vortex dynamics in three-dimensional continuous myocardium with fiber rotation: filament instability and fibrillation *Chaos* **8** 20–47

Fish J M and Antzelevitch C 2003 Cellular and ionic basis for the sex-related difference in the manifestation of the brugada syndrome and progressive conduction disease phenotypes *J. Electrocardiol.* **36** 173–9

FitzHugh R 1960 Thresholds and plateaus in the Hodgkin–Huxley nerve equations *J. Gen. Physiol.* **43** 867–96

FitzHugh R 1961 Impulses and physiological states in theoretical models of nerve membrane *Biophys. J.* **1** 445–66

Garfinkel A, Kim Y H, Voroshilovsky O, Qu Z, Kil J R, Lee M H, Karagueuzian H S, Weiss J N and Chen P S 2000 Preventing ventricular fibrillation by flattening cardiac restitution *Proc. Natl. Acad. Sci. USA* **97** 6061–6

Grant A O 2001 Molecular biology of sodium channels and their role in cardiac arrhythmias *Am. J. Med.* **110** 296–305

Iost N, Virag L, Opincariu M, Szecsi J, Varro A and Papp J G 1998 Delayed rectifier potassium current in undiseased human ventricular myocytes *Cardiovasc. Res.* **40** 508–15

Iyer V, Mazhari R and Winslow R L 2004 A computational model of the human left-ventricular epicardial myocyte *Biophys. J.* **87** 1507–25

Karma A 1993 Spiral breakup in model equations of action potential propagation in cardiac tissue *Phys. Rev. Lett.* **71** 1103–6

Karma A 1994 Electrical alternans and spiral wave breakup in cardiac tissue *Chaos* **4** 461–72

Keener J and Sneyd J 1998 *Mathematical Physiology* (Berlin: Springer)

Keller D I, Acharfi S, Delacretaz E, Benammar N, Rotter M, Pfammatter J, Fressart V, Guicheney P and Chahine M 2003 A novel mutation in scn5a, delqko 1507-1509, causing long qt syndrome; role of q1507 residue in sodium channel inactivation *J. Mol. Cellular Cardiol.* **35** 1513–21

Koller M L, Riccio M L and Gilmour R F Jr 2000 Effects of [K(+)](o) on electrical restitution and activation dynamics during ventricular fibrillation *Am. J. Physiol. Heart Circ. Physiol.* **279** H2665–72

Li G R, Feng J, Yue L and Carrier M 1998 Transmural heterogeneity of action potentials and I_{to1} in myocytes isolated from the human right ventricle *Am. J. Physiol. Heart Circ. Physiol.* **275** H369–77

Li G R, Feng J, Yue L, Carrier M and Nattel S 1996 Evidence for two components of delayed rectifier K^+ current in human ventricular myocytes *Circ. Res.* **78** 689–96

Luo C and Rudy Y 1991 A model of the ventricular cardiac action potential, depolarization, repolarization, and their interaction *Circ. Res.* **68** 1501–26

Luo C and Rudy Y 1994 A dynamic model of the cardiac ventricular action potential I simulations of ionic currents and concentration changes *Circ. Res.* **74** 1071–96

Nabauer M, Beuckelmann D J, Uberfuhr P and Steinbeck G 1996 Regional differences in current density and rate-dependent properties of the transient outward current in subepicardial and subendocardial myocytes of human left ventricle *Circulation* **93** 168–77

Nagumo J S, Arimoto S and Yoshizawa S 1962 An active pulse transmission line simulating nerve axon *Proc. IRE* **50** 2061–71

Nash M P, Bradley C P, Sutton P M, Clayton R H, Kallis P, Hayward M, Paterson D J and Taggart P 2006 Whole heart APD restitution properties in cardiac patients: a combined clinical and modeling study *Exp. Physiol.* **91** 339–54

Noble D, Varghese A, Kohl P and Noble P 1998 Improved guinea-pig ventricular cell model incorporating a diadic space, I_{Kr} and I_{Ks}, and length- and tension-dependent processes *Can. J. Cardiol.* **14** 123–34

Panfilov A V and Holden A V 1990 Self-generation of turbulent vortices in a two-dimensional model of cardiac tissue *Phys. Lett.* A **147** 463–6

Pereon Y, Demolombe S, Baro I, Drouin E, Charpentier F and Escande D 2000 Differential expression of KvLQT1 isoforms across the human ventricular wall *Am. J. Physiol. Heart Circ. Physiol.* **278** H1908–15

Priebe L and Beuckelmann D J 1998 Simulation study of cellular electric properties in heart failure *Circ. Res.* **82** 1206–23

Qu Z, Weiss J N and Garfinkel A 1999 Cardiac electrical restitution properties and stability of reentrant spiral waves: a simulation study *Am. J. Physiol. Heart Circ. Physiol* **276** H269–83

Riccio M L, Koller M L and Gilmour R F Jr 1999 Electrical restitution and spatiotemporal organization during ventricular fibrillation *Circ. Res.* **84** 955–63

Rice J J, Jafri M S and Winslow R L 1999 Modeling gain and gradedness of Ca^{2+} release in the functional unit of the cardiac diadic space *Biophys. J.* **77** 1871–84

Rivolta I, Abriel H, Tateyama M, Liu H, Memmi M, Vardas P, Napolitano C, Priori S G and Kass R S 2001 Inherited brugada and long QT-3 syndrome. Mutations of a single residue of the cardiac sodium channel confer distinct channel and clinical phenotypes *J. Biol. Chem.* **276** 30623–30

Rush S and Larsen H 1978 A practical algorithm for solving dynamic membrane equations *IEEE Trans. Biomed. Eng.* **25** 389–92

Taggart P, Sutton P M I, Opthof T, Coronel R, Trimlett R, Pugsley W and Kallis P 2000 Inhomogeneous transmural conduction during early ischemia in patients with coronary artery disease *J. Mol. Cell. Cardiol.* **32** 621–39

Ten Tusscher K H W J, Noble D, Noble P J and Panfilov A V 2004 A model for human ventricular tissue *Am. J. Physiol. Heart Circ. Physiol.* **286** H1573–89

TenTusscher K H W J and Panfilov A V 2004 Eikonal formulation of the minimal principle for scroll wave filaments *Phys. Rev. Lett.* **93** 108106-1–108106-4

Ten Tusscher K H W J and Panfilov A V 2006 Alternans and spiral breakup in a human ventricular tissue model *Am. J. Physiol. Heart Circ. Physiol.* **291** H1088–100

Wei J, Wang D W, Alings M, Fish F, Wathen M, Roden D M and George A L 1999 Congenital long-qt syndrome caused by a novel mutation in a conserved acidic domain of the cardiac na+ channel *Circulation* **99** 3165–71

Wettwer E, Amos G J, Posival H and Ravens U 1994 Transient outward current in human ventricular myocytes of subepicardial and subendocardial origin *Circ. Res.* **75** 473–82

Winslow R L, Rice J, Jafri S, Marban E and O'Rourke B 1999 Mechanisms of altered excitation-contraction coupling in canine tachycardia-induced heart failure, II Model studies *Circ. Res.* **84** 571–86

Xie F, Qu Z, Garfinkel A and Weiss J N 2001 Effects of simulated ischemia on spiral wave stability *Am. J. Physiol. Heart Circ. Physiol.* **280** H1667–73

Zeng J, Laurita K R, Rosenbaum D S and Rudy Y 1995 Two components of the delayed rectifier K^+ current in ventricular myocytes of the guinea pig type. Theoretical formulation and their role in repolarization *Circ. Res.* **77** 140–52

Zhang H, Holden A V, Kodama I, Honjo H, Lei M, Varghese T and Boyett M R 2000 Mathematical models of action potentials in the periphery and center of the rabbit sinoatrial node *Am. J. Physiol. Heart Circ. Physiol.* **279** H397–421